Iron complexes as electrocatalysts for the water oxidation reaction

Kottrup, K.G.

Chapter 4

Electrochemical versus chemical oxidation – re-evaluating the benchmark water oxidation catalyst α-[Fe(bpmcn)(OTf)$_2$] via electroanalytical methods

*The complex α-[Fe(bpmcn)(OTf)$_2$] (**1**) (with bpmcn = N,N'-dimethyl-N,N'-bis(2-pyridylmethyl)-cyclohexane-1,2-diamine) was first reported in 2011 by Fillol et. al as an active iron-based catalyst for the water oxidation reaction. It has since taken on a status as a benchmark system for iron-based water oxidation catalysis. In this chapter we describe the results of electroanalytical investigations of complex **1**, complex **2** – the D$_4$-analogue in which the benzylic hydrogen atoms in the structure have been replaced with deuterium – and the non-deuterated Fe^{III} analogue complex **3**. The reactivity of these complexes for water oxidation under electrochemical conditions is compared to their activity under chemically driven conditions, in particular with respect to the difference in stability between complex **1** and the D$_4$ analogue **2**, which was observed in the presence of excess Cerium(IV). While the results show that all three complexes are active for water oxidation at potentials ≥1.8 V vs. RHE, their performance is not exceptional compared to other iron-based electrocatalysts. Furthermore, no significant difference was found between complex **1** and **2** in terms of stability during electrocatalysis. Finally, complexes **1** and **2** were studied with different electrode materials and demonstrated a much more complicated behaviour in combination with a gold working electrode compared to a pyrolytic graphite working electrode. The underlying reasons for this behaviour are not yet fully understood.*

The results presented in this chapter are to be submitted as a full paper: *manuscript in preparation*.

4.1 Introduction

In 2011 Fillol and co-workers published a much-noticed report on iron-based homogeneous water oxidation catalysts.[1] The catalyst which the best performance in their screening library was α-[Fe(bpmcn)$(OTf)_2$] (**1**) (with bpmcn = *N*,*N*'-dimethyl-*N*,*N*'-bis(2-pyridylmethyl)-cyclohexane-1,2-diamine) which in the presence of excess cerium(IV) ammonium nitrate (CAN) produced O_2 with turnover numbers of about 360 and an initial-rate turnover frequency of 0.23 s^{-1}. When periodate was used instead of CAN, turnover numbers of >1050 were reported albeit at a lower rate of 0.06 s^{-1}. While these results are very promising, the stability of the catalyst still needs to be improved to yield higher TONs in order to make the transition from a proof of concept to an actual application.

In 1994 Collins studied the degradation pathways of metal complexes in high oxidation states, developing a set of rules regarding the ligand structure for the design of transition metal complexes to be used under strongly oxidative conditions.[2] One of the rules he established is that hydrogen atoms in β-position to heteroatom donors should be avoided as β-hydrogen elimination can occur, resulting in degradation of the ligand. The translation of his findings into the design of a new catalyst resulted in development of the tetra-amido macrocyclic ligand system (TAML) which was subsequently successfully used in water oxidation chemistry.[3] The most active Fe-TAML complex that was found in the study (Fig. 4.1) had a remarkably high turnover frequency of 1.3 s^{-1}. However, despite following the rules established previously, the catalytic activity of the Fe-TAML catalyst was short-lived with only 16 turnovers.

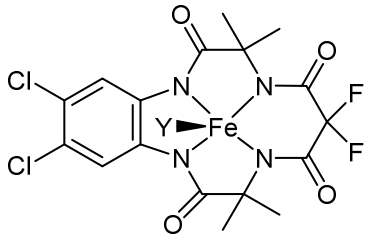

Figure 4.1: Structure of the most active Fe-TAML complex reported by Collins et al. (Y = H_2O)[3]

Following their initial report, Fillol and co-workers made efforts to identify and eliminate deactivation pathways of complex **1** to improve the catalyst lifetime. One of the major weaknesses that was identified in the structure of the complex are the benzylic –CH_2– hydrogen atoms, which is in agreement with the rules

established by Collins. They open up a pathway resulting in the loss of one or both of the pyridyl groups, leading to deactivation of the catalyst.[4] By replacing the benzylic protium atoms with deuterium atoms, the authors were able to demonstrate an increase of the turnover number by a factor of 4-5 under the same conditions without affecting the turnover frequency.[4] This indicates that the mechanism of the catalytic reaction remains the same while the stability of the catalyst is improved.

Because of these very promising results we decided to investigate complex **1** and the deuterated analogue D_4-α-[Fe(bpmcn)$(OTf)_2$] (**2**) (Fig. 4.2) using electroanalytical techniques to determine whether a similar effect of the deuteration on the catalyst lifetime can be seen in electrocatalytic applications. Since complexes **1** and **2** were found to undergo rapid ligand de-coordination in low pH aqueous media, the electrochemistry of both complexes was studied in $NaClO_4$ electrolyte solutions. The Fe^{III} analogue α-[Fe(bpmcn)Cl_2]Cl (**3**) with protium in the backbone and bearing chloride ligands instead of triflate ligands (Fig. 4.2) was found to be substantially more stable under acidic conditions and was thus also used for electrochemical experiments in acidic media.

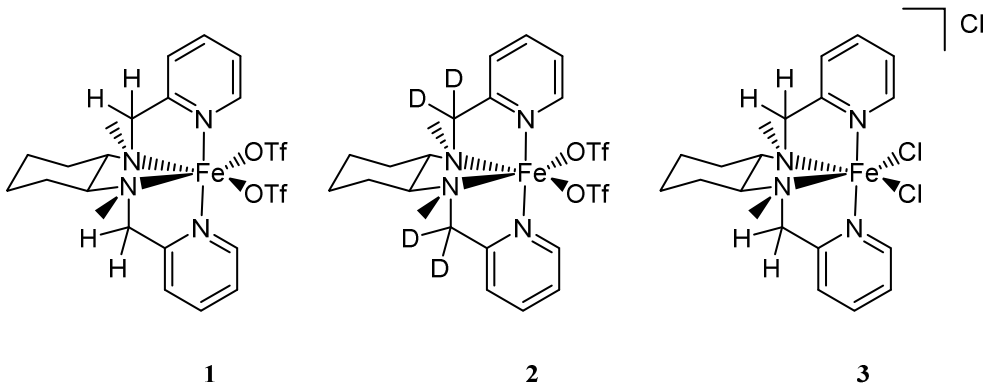

1 **2** **3**

Figure 4.2: Structures of complexes **1**, **2** and **3**

4.2 Results

*4.2.1 Stability of complexes **1-3** in solution under different pH conditions*

Considering the harsh conditions of the previously reported experiments involving CAN (pH ≤ 1), complexes **1** and **2** were initially studied in 0.1 M $HClO_4$ electrolyte solutions. Cyclic voltammetry (CV) experiments yielded identical results for both complexes. The voltammograms of both complexes initially look as expected,

showing a reversible Fe^{II}/Fe^{III} redox couple at 0.8 V vs. RHE (Fig. 4.3). However, follow-up voltammograms which were recorded 3-4 hours later show in both cases a current profile which is significantly different from the one that was recorded initially (Fig. 4.4).

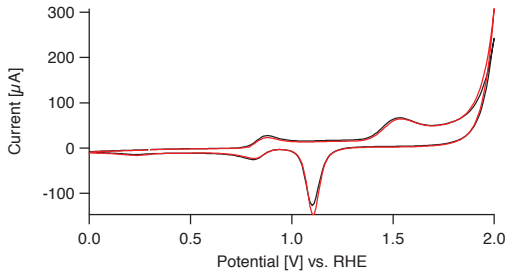

Figure 4.3: Initial voltammograms of 1.1 mM solutions of complexes **1** (red) and **2** (black) in 0.1 M $HClO_4$. Both voltammograms were recorded with a gold working electrode, scanning between 0.0 and 2.0 V vs. RHE at 100 mV/s, starting at 0.3 V vs. RHE.

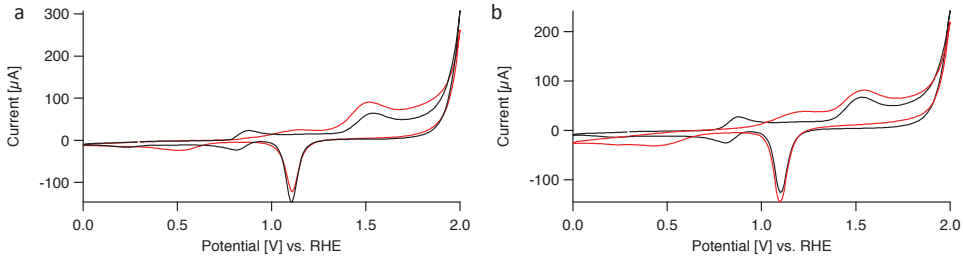

Figure 4.4: Voltammograms of (a) 1.1 mM solutions of complexes **1** in 0.1 M $HClO_4$ at t = 0 h (black) and after 3 h (red) and (b) 1.1 mM solutions of complexes **2** in 0.1 M $HClO_4$ at t = 0 h (black) and after 3.5 h (red). All voltammograms were recorded with a gold working electrode, scanning between 0.0 and 2.0 V vs. RHE at 100 mV/s, starting at 0.3 V vs. RHE.

The disappearance of the Fe^{II}/Fe^{III} redox couple over time indicates deterioration of the complex in both cases which is in agreement with previous reports which described that complexes **1** and **2** are unstable in solutions of 0.1 M triflic acid.[5-6] The deterioration of the complexes was also accompanied by the visible build-up of a flocculent white precipitate in the electrochemical cell (Fig. C.1, Appendix C). Accordingly, the UV-vis absorption spectrum of complex **2** in 0.1 M $HClO_4$ (Fig. 4.5) shows changes on the time scale of minutes after the initial dissolution of the complex: the absorption band around 370 nm disappears while the peak at 260 nm increases with time. The decrease of the band at 370 nm has previously been attributed to the disappearance of MLCT transitions as the ligand dissociates from the metal centre while the increase of the peak at 260 nm has been attributed to a π–π* transition in the ligand which is more intense in the free

ligand compared to the coordinated ligand.[5] In a 0.1 M $NaClO_4$ solution, the UV-vis absorption spectrum of complex **2** was found to be stable with no visible changes over several hours (Fig. 4.6).

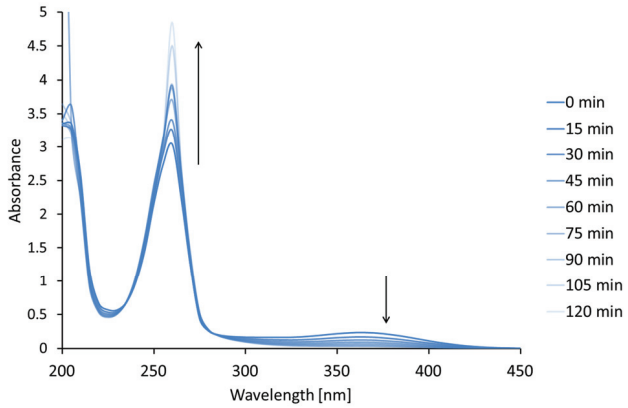

Figure 4.5: Evolution of the UV-vis absorption of complex **2** in a 0.1 M $HClO_4$ solution over 2 h, recorded in 15 min intervals.

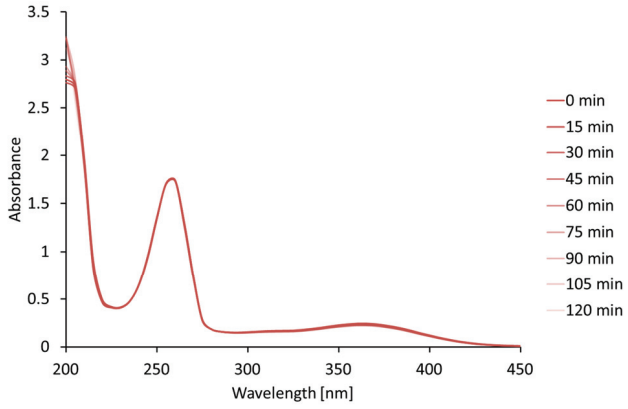

Figure 4.6: Evolution of the UV-vis absorption of complex **2** in a 0.1 M $NaClO_4$ solution over 2 h, recorded in 15 min intervals.

Based on the combined results of the UV-vis and CV experiments with complexes **1** and **2**, it seems clear that both complexes are unstable in solution at low pH and stable for several hours in an unbuffered electrolyte solution.

Since complex **3** was found to dissolve poorly in solutions containing perchlorate ions, 0.1 M H_2SO_4 and 0.1 M Na_2SO_4 were chosen as the appropriate electrolyte media instead even though the sulfate ion has been shown to inhibit catalytic activity slightly compared to the perchlorate ion in some cases.[7] In contrast to complexes **1** and **2**, complex **3** was found to be stable under both acidic and

neutral conditions. UV-vis absorption experiments show that complex **3** is stable in both 0.1 M H_2SO_4 and 0.1 M Na_2SO_4 for several hours with no change in the observed spectra (Fig. 4.7-4.8). The results indicate that iron in the oxidation state +III binds the bpmcn ligand stronger than iron in the oxidation state +II, resulting in a complex which is more stable in acidic media.

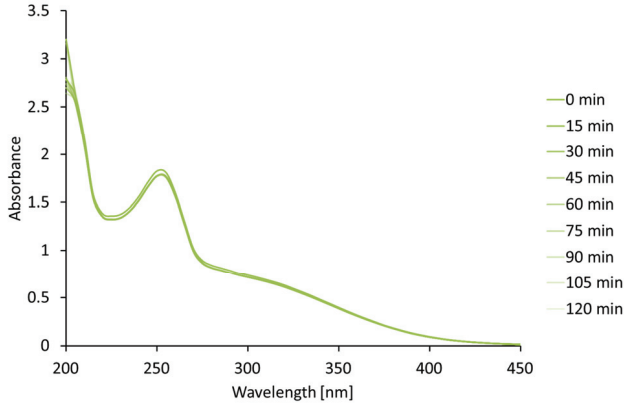

Figure 4.7: Evolution of the UV-vis absorption of complex **3** in a 0.1 M H_2SO_4 solution over 2 h, recorded in 15 min intervals.

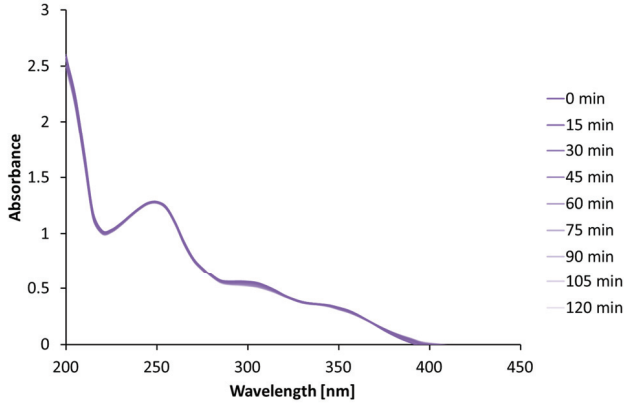

Figure 4.8: Evolution of the UV-vis absorption of complex **3** in a 0.1 M Na_2SO_4 solution over 2 h, recorded in 15 min intervals.

*4.2.2 Electrochemistry of complexes **1** and **2***

4.2.2a Cyclic voltammetry

Based on the results described in section 4.2.1, $NaClO_4$ was selected as the appropriate electrolyte for electrochemical experiments with complexes **1** and **2**. To determine any possible influence of the electrode material on the observed electrochemistry, working electrodes made from gold and pyrolytic graphite (PG) were used.

In all cyclic voltammetry experiments, complexes **1** and **2** show virtually identical behaviour. Using a gold working electrode, both complexes show a reversible Fe^{II}/Fe^{III} redox couple at 0.9 V which is followed by two oxidation waves, labeled I and II, between 1.5 and 1.9 V (Fig. 4.9) which are assigned to the formation of gold oxide at the surface of the working electrode (see section 4.2.2b). At about 1.9 V the onset of another oxidative wave is seen which could potentially indicate catalytic current. In the backward scan, a reduction wave at 1.2 V is visible which corresponds to the reduction of the oxidized electrode surface from gold oxide back to gold.

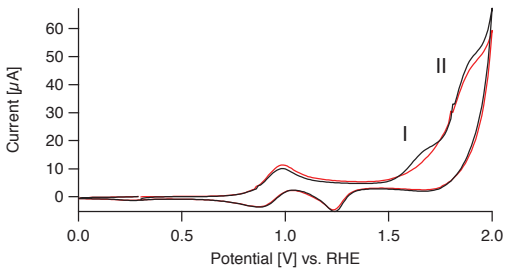

Figure 4.9: Voltammograms of 1.1 mM solutions of complexes **1** (red) and **2** (black) in 0.1 M $NaClO_4$. Both CVs were recorded with a gold working electrode, scanning between 0.0 and 2.0 V vs. RHE at 10 mV/s, starting at 0.3 V vs. RHE

In the first scan of the CV experiment, the current starting at 1.9 V beyond the gold oxidation waves I and II is small. A significant increase in the peak current at 2.0 V was found in subsequent scans when cycling the potential between 0.0 and 2.0 V at a scan rate of 10 mV/s (Fig. 4.10). Long-term experiments under these conditions show that for complex **1** the maximum current at 2.0 V is reached after 27 scans with most of the increase already taking place during the first few scans (Fig. 4.11a and Table 4.1). While the current at 2.0 V increased significantly over several scans, the current of the redox couple remained largely unaffected (Fig. 4.11b and Table 4.1). This is a clear indication that the complexes remain largely

intact during the experiment, meaning that the increase in peak current is unlikely to be due to the formation of a different homogeneous catalytically active species from complexes **1** and **2**.

In CV experiments with a PG working electrode, complexes **1** and **2** show again a reversible Fe^{II}/Fe^{III} redox couple at 0.9 V (Fig. 4.12) as was previously seen with a gold working electrode. Beyond that, only a single irreversible oxidation wave starting at about 1.5 V can be seen in the voltammogram of complexes **1** and **2** recorded with a PG working electrode.

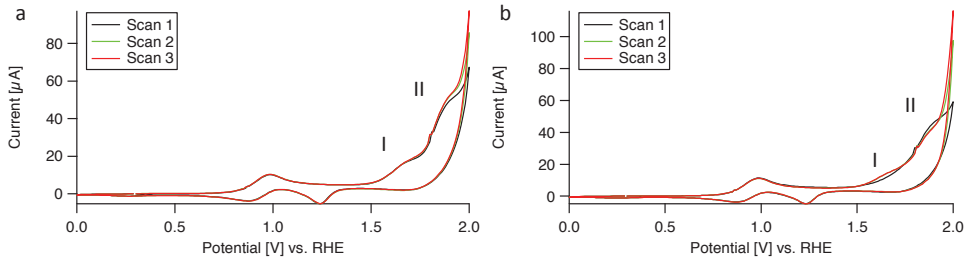

Figure 4.10: Voltammograms of 1.1 mM complex **2** (a) and 1.1 mM complex **1** (b) recorded with a gold working electrode in a 0.1 M $NaClO_4$ solution. Shown are 3 subsequent scans recorded between 0.0 and 2.0 V vs. RHE at a scan rate of 10 mV/s, starting each scan at 0.3 V vs. RHE.

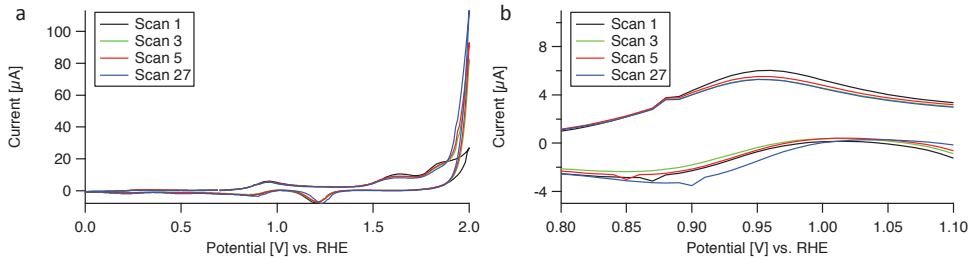

Figure 4.11: Scans 1, 3, 5 and 27 of a CV experiment of 1.1 mM complex **1** in a 0.1 M $NaClO_4$ solution, scanning between 0.0 and 2.0 V vs. RHE at a scan rate of 10 mV/s, starting at 0.7 V vs. RHE. (a) Full CV between 0.0 and 2.0 V vs. RHE (b) Magnification of the area between 0.8 and 1.1 V vs. RHE to highlight the $Fe^{II/III}$ redox couple.

Table 4.1: Values of the current recorded for the $Fe^{II/III}$ transition and the peak at 2.0 V vs. RHE for selected scans during a long-term CV experiment with complex **1**, corresponding to Fig. 4.11.

Scan #	Peak current $Fe^{II/III}$ [µA]	Peak current at 2.0 V [µA]
1	6	27
3	5	83
5	6	93
27	5	113

Conditions: Gold working electrode, 1.1 mM complex **1**, 0.1 M $NaClO_4$, scan range: 0.0-2.0 V vs. RHE, scan rate: 10 mV/s

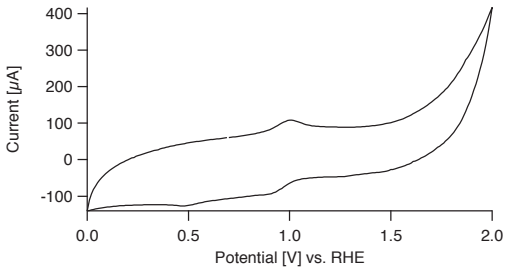

Figure 4.12: Voltammogram of 1.1 mM complex **1** in a 0.1 M $NaClO_4$ solution recorded with a PG working electrode at a scan rate of 100 mV/s between 0.0 and 2.0 V vs. RHE, starting at 0.7 V vs. RHE.

4.2.2b On-line electrochemical mass spectrometry

To assess the water oxidation capabilities of complexes **1** and **2**, on-line electrochemical mass spectrometry (OLEMS) experiments were carried out in combination with cyclic voltammetry. In OLEMS measurements, the *m/z* traces for selected gaseous products, sampled close to the electrode surface in solution, are recorded during electrochemical measurements.[8] During all OLEMS experiments, *m/z* = 32 was recorded to monitor oxygen evolution while *m/z* = 44 was recorded to monitor any CO_2 formation as a result of potential oxidative decomposition of the ligand under strongly oxidizing conditions.[9-12] In all OLEMS experiments discussed in this chapter, the potential was cycled between 1.3 and 2.0 V at 1 mV/s for a total of three cycles.

In OLEMS experiments with a PG working electrode, complex **1** demonstrates persistent water oxidation activity across all three scans (Fig. 4.13). In the corresponding current trace (Fig. 4.13, bottom), oxidative current can be seen starting at 1.5 V with a sharp increase in current at about 1.8 V. These features in the current trace are consistent with the results previously seen in the CV experiment, recorded between 0.0 and 2.0 V with a PG working electrode in the presence of complex **1** (Fig. 4.12). The mass traces for O_2 and CO_2 measured during the OLEMS experiment show onsets that correspond well with the onsets in the current trace. O_2 evolution starts at 1.8 V while CO_2 formation starts already at lower potentials around 1.5 V. The formation of CO_2 could indicate decomposition of the complex. However, similar CO_2 formation behaviour with an onset at potentials below the onset of oxygen evolution is routinely detected in OLEMS experiments with a PG working electrode for all metal complexes described in this thesis and even – albeit to a lesser extent – in the absence of any metal complex in solution (cf. chapter 5).

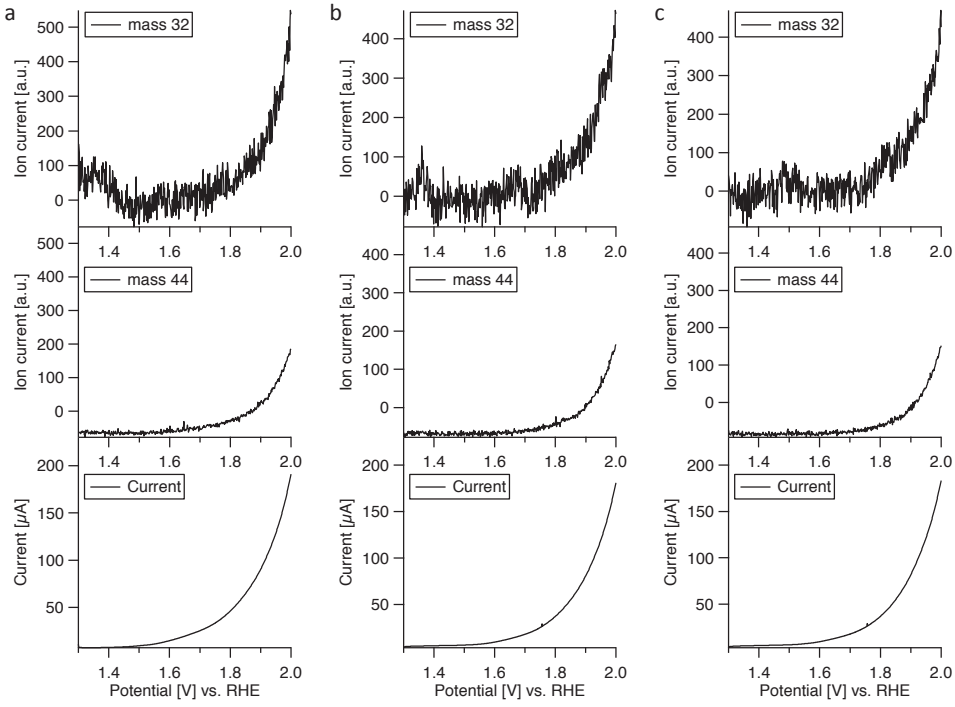

Figure 4.13: OLEMS measurement of 1.1 mM complex **1** in a 0.1 M $NaClO_4$ solution using a PG working electrode, recorded while cycling the potential between 1.3 and 2.0 V vs. RHE, starting at 1.3 V vs. RHE at a scan rate of 1 mV/s. Depicted are the *m/z* traces of O_2 (top), CO_2 (middle) and the corresponding current (bottom). (a) scan 1 (b) scan 2 (c) scan 3. For the sake of clarity only the forward scan of each experiment is shown.

OLEMS experiments of complexes **1** and **2** in combination with a gold working electrode instead of a PG electrode yield more complicated results. During the second and third scan of each OLEMS experiment with a gold working electrode, both complexes show again stable water oxidation activity as was previously seen in the OLEMS experiment of complex **1** with a PG working electrode. In contrast to that, both complexes show identical initial behaviour during the first scan of the OLEMS experiment with a gold working electrode, which differs substantially from their behaviour during the second and third scan. For the sake of structuring the discussion, the second and third scan of the OLEMS experiments of both complexes are discussed first, followed by a discussion of the first scan.

In the second and third scan of the OLEMS experiments, a sharp increase in the recorded current is visible, starting between 1.8 and 1.9 V. The mass traces for *m/z* = 32 shows an onset of oxygen evolution which correlates with the oxidative current while the mass traces for *m/z* = 44 show no signs of CO_2 formation (Fig. 4.14 and Fig. 4.15). The onset of oxygen formation appears to be slightly delayed

in the OLEMS experiments with a gold working electrode compared to the experiments with a PG working electrode. However, the contribution of CO_2 formation to the current in the experiment with a PG electrode makes it more difficult to determine the onset of oxygen evolution for the experiment with PG. The lack of CO_2 formation in the experiment with gold on the other hand indicates that that the CO_2 formation observed for the case of a PG working electrode is mainly due to oxidation of the electrode material itself.

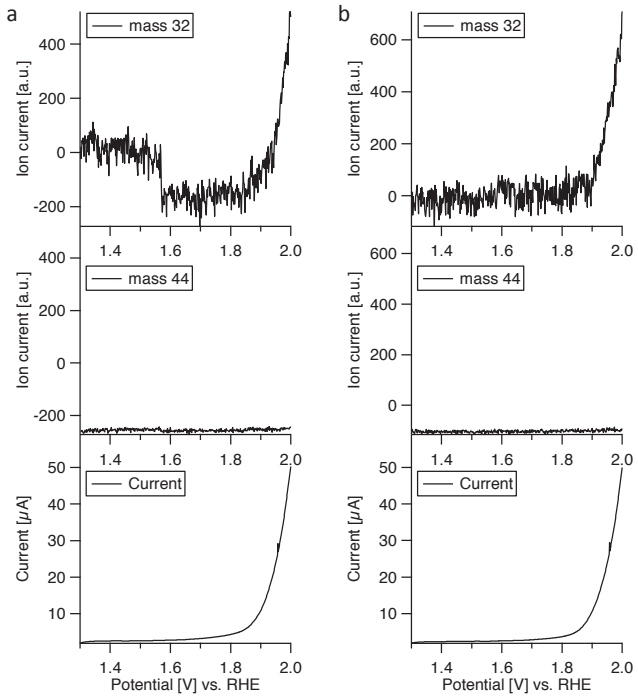

Figure 4.14: Results of the second (a) and the third (b) scan of an OLEMS experiment recorded during potential cycling with complex **1** using a gold working electrode. Conditions: 1.1 mM complex **1**, 0.1 M $NaClO_4$, scan range: 1.3-2.0 V vs. RHE, starting at 1.3 V vs. RHE, scan rate 1 mV/s. Depicted are the *m/z* traces of O_2 (top) CO_2 (middle) and the corresponding current (bottom). For the sake of clarity, only the forward scan of each experiment is shown.

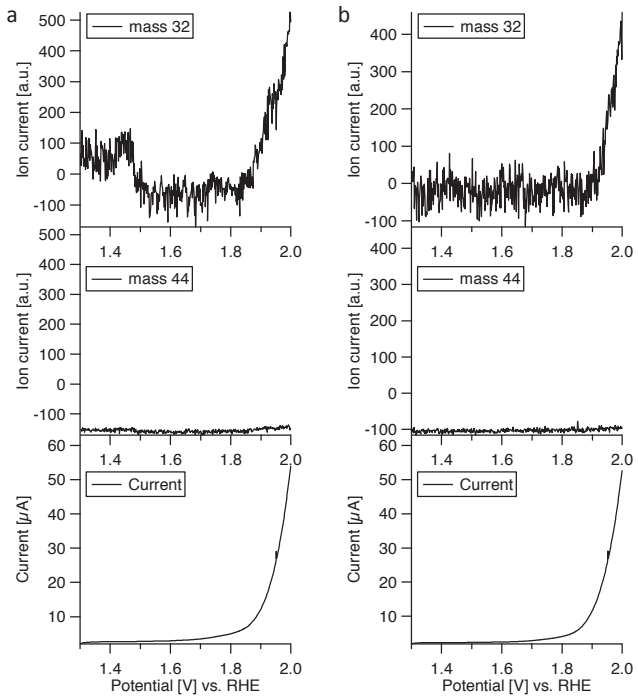

Figure 4.15: Results of the second (a) and the third (b) scan of an OLEMS experiment recorded during potential cycling with complex **2** using a gold working electrode. Conditions: 1.1 mM complex **2**, 0.1 M $NaClO_4$, scan range: 1.3-2.0 V vs. RHE, starting at 1.3 V vs. RHE, scan rate 1 mV/s. Depicted are the *m/z* traces of O_2 (top) CO_2 (middle) and the corresponding current (bottom). For the sake of clarity, only the forward scan of each experiment is shown.

In contrast to the results just described for the second and third scan of the OLEMS experiments with a gold working electrode, the results of the first scan of each OLEMS experiment are significantly different. This holds true for the mass traces and the current profile. During the first scan, the mass traces for *m/z* = 44 show that small quantities of CO_2 are being formed with an onset of 1.8 V while the mass traces for *m/z* = 32 indicate that oxygen is formed already at potentials as low as 1.6 V (Fig. 4.16, top and middle). The current that was measured during the first scan (Fig. 4.16, bottom) shows the same profile that was observed during previous CV experiments of complexes **1** and **2** with a gold working electrode, discussed in section 4.2.2a (Fig. 4.9-4.11). Starting at about 1.5 V, the two oxidation waves I and II can be seen, followed by a sharp increase in current at 1.9 V. The signal of the O_2 mass trace in figure 4.16 appears to follow the oxidative current which suggests that the current might be related to oxygen evolution. However, it is expected that the oxidation of the gold surface to gold oxide contributes significantly to the recorded current during the first scan as the

surface of the gold working electrode is not yet oxidized to gold oxide at the start of experiment.

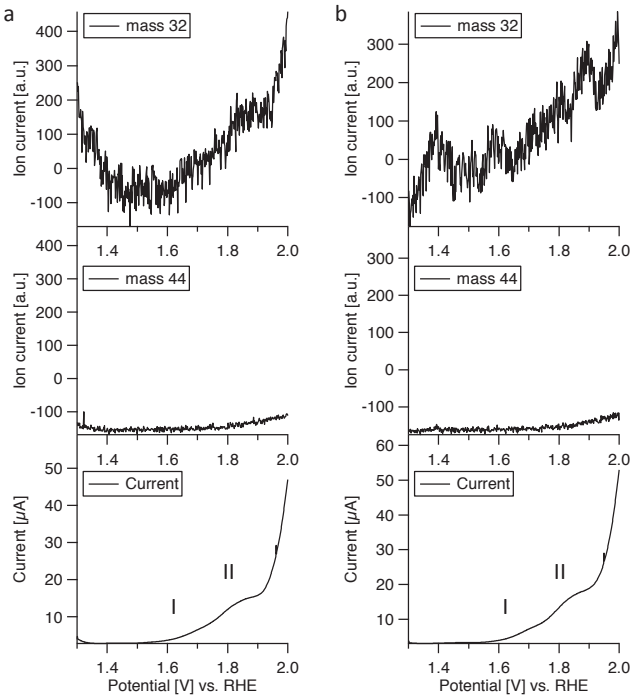

Figure 4.16: Results of the first scans of an OLEMS experiment with (a) complex **1** and (b) complex **2**, recorded during potential cycling with complex **1** using a gold working electrode. Conditions: 1.1 mM complex **1**/**2**, 0.1 M $NaClO_4$, scan range: 1.3-2.0 V vs. RHE, starting at 1.3 V vs. RHE, scan rate 1 mV/s. Depicted are the *m/z* traces of O_2 (top) CO_2 (middle) and the corresponding current (bottom). For the sake of clarity, only the forward scan of each experiment is shown.

To disentangle contributions of the complexes from contributions of gold oxide formation to the current, two back-to-back CV experiments were carried out with complex **2**. Both experiments were recorded under the same conditions as the OLEMS experiment described in figures 4.14-4.16 by cycling the potential several times between 1.3 and 2.0 V at 1 mV/s. Between both experiments, the connection between the working electrode and the electrolyte was broken and subsequently re-established after brief mixing of the electrolyte solution to ensure exposure of the electrode to new, unreacted complex for the second experiment. During this entire procedure, the resting potential at the working electrode was kept at 1.3 V.

Since the surface of the gold working electrode is not yet oxidized to gold oxide at the start of the first CV experiment, the current associated with the formation of

gold oxide should contribute to the current profile of the first scan of the first experiment. By keeping the potential at the working electrode greater or equal to 1.3 V throughout the entire procedure, the reduction of the formed gold oxide is prevented. Therefore no current from gold oxide formation should be present in the voltammogram of any of the subsequent scans of the procedure. If the two current waves I and II in the first scan of the OLEMS experiment are caused by the formation of gold oxide, they should therefore only appear in the first scan of the first experiment. Additionally, the current of the first and second scan of the first experiment should differ, due to the contribution of gold oxide to the first scan, while the current of the first and second scan of the second experiment should be identical. If, on the other hand, oxidation reactions of complexes **1** and **2** contribute to the current profile of the first scan of the OLEMS experiment (Fig. 4.16, bottom), it is expected that the current profile will change from the first to the second scan in the second CV experiment as well.

The results of the first CV experiment (Fig. 4.17a) clearly show that, as expected, waves I and II are present in the first scan and absent in the second scan, as was previously seen in the OLEMS experiments. In the second CV experiment, however, waves I and II are absent and the current profiles of the first and second scan are identical (Fig. 4.17b).

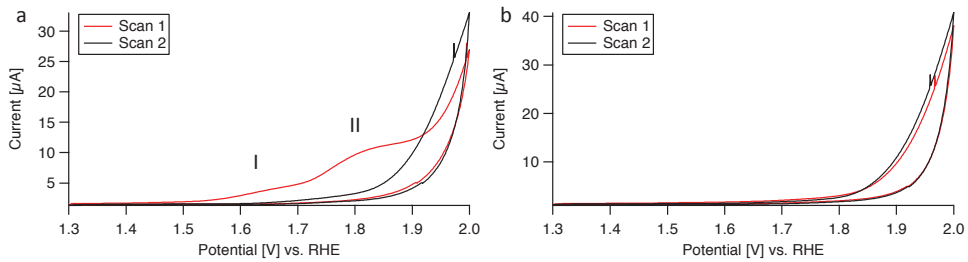

Figure 4.17: Results of two consecutive CV experiments with complex **2**, recorded with a gold working electrode in the presence of 1.1 mM complex **2** in a 0.1 M $NaClO_4$ solution, scanning between 1.3 and 2.0 V vs. RHE at a scan rate of 1 mV/s, starting each scan at 1.3 V vs. RHE. After scanning between 1.3 and 2.0 V at 1 mV/s for three cycles, the meniscus at the electrode/electrolyte interface was broken and subsequently re-formed after homogenization of the electrolyte solution to ensure exposure of the electrode to new, unreacted complex **2**. This was followed by another CV experiment between 1.3 and 2.0 V at 1 mV/s for two cycles. The resting potential at the working electrode was kept at 1.3 V throughout the entire procedure to avoid gold oxide reduction. (a) First and second scan of the first CV experiment. (b) First and second scan of the second CV experiment. For both experiments, the first scan is depicted in red while the second scan is depicted in black.

The absence of waves I and II in both scans of the second CV experiment confirms that the oxidative current is not an inherent property of complexes **1** and **2** but

instead most likely related to the formation of gold oxide at the surface of the electrode.

The amounts of O_2 that are being detected during the OLEMS experiment shown in figure 4.16 are close to the lower detection limit of the system. Therefore, it is difficult to confidently distinguish actual signals from the artefacts which are commonly present in the mass traces of some OLEMS measurements. Some examples of such artefacts are highlighted in figures C.2 and C.3 in appendix C. This raises the question whether the oxygen evolution behaviour that was observed during the first scan of each OLEMS experiment is actually indicative of a real signal or random noise instead. Therefore the OLEMS experiments of complexes **1** and **2** with a gold working electrode were carried out in duplicate with the second experiment taking place on a different day. The results show that although artefacts obscure the real features to some extent, the same qualitative oxygen evolution behaviour does indeed persist across experiments (Fig. 4.18).

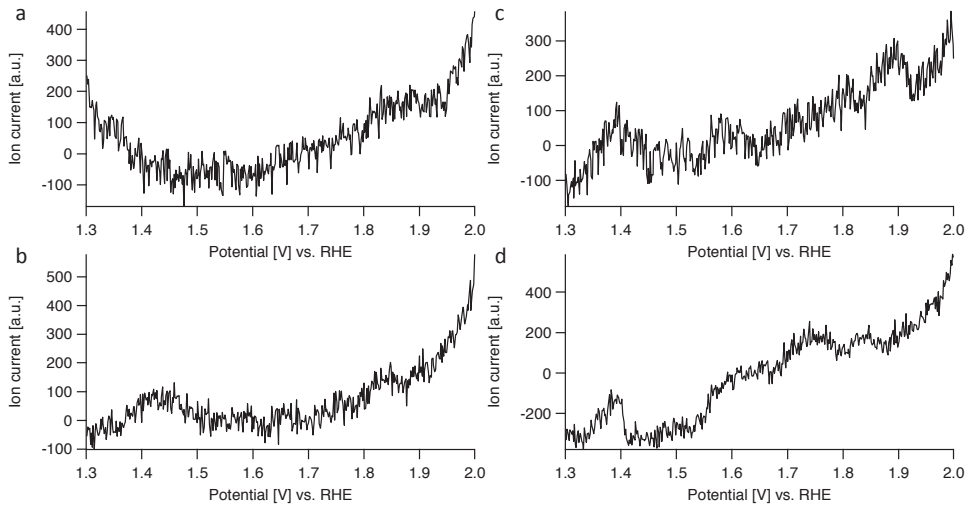

Figure 4.18: Results of several OLEMS experiments of complexes **1** and **2**. Depicted are the *m/z* traces for O_2 of the respective first of each experiment, recorded while cycling the potential between 1.3 and 2.0 V vs. RHE with a gold working electrode in a 0.1 M $NaClO_4$ solution at a scan rate of 1 mV/s, starting each scan at 1.3 V vs. RHE. (a) 1.1 mM complex **1**, first experiment (b) 1.1 mM complex **1**, second experiment (c) 1.1 mM complex **2**, first experiment (d) 1.1 mM complex **2**, second experiment. In all cases only the forward scan of each experiment is shown for the sake of clarity.

4.2.2c Electrochemical quartz crystal microbalance experiments

The results of CV experiments with both complexes **1** and **2**, using a gold working electrode, showed an increasing peak current at 2.0 V during repeated potential cycling between 0.0 and 2.0 V. This observation suggests that an activation of the catalyst takes place during repeated potential cycling. One possible explanation might be the formation of a catalytically active heterogeneous species at the surface of the working electrode at high potentials since heterogeneous iron-based materials such as Fe_2O_3 are known to be active water oxidation catalysts.[13-16] Therefore the potential formation of catalytically active heterogeneous materials is a constant concern in the field of homogeneous water oxidation catalysis.[10]

The fact that the $Fe^{II/III}$ redox couple remains largely unchanged while the peak current at 2.0 V increases during CV experiments already offers some evidence that the increase in current is not related to the decomposition of the complex. Nevertheless, electrochemical quartz crystal microbalance (EQCM) experiments were carried out in order to obtain direct information about the formation of any surface deposits.[17-18] The working electrode in EQCM experiments consists of a thin layer of gold, deposited on a quartz crystal oscillator. Mass changes at the working electrode can be detected by measuring changes in the resonance frequency of the quartz crystal. To avoid damaging the thin gold layer of the EQCM electrode and due to the mass change associated with gold oxide formation and reduction, the potential was kept above 1.3 V at all times during EQCM experiments to avoid gold oxide reduction.

Figure 4.19 shows the results of an EQCM experiment between 1.3 and 2.0 V at 1 mV/s, recorded with a gold working electrode in the presence of complex **1**. During the first scan of the experiment (Fig. 4.19a), an increase in the vibration frequency can be seen, as is evident from a positive Δ(frequency) response. This response translates to an apparent decrease in the mass of the electrode. This seemingly strange observation has previously been attributed to bubble formation at the working electrode.[17] After the initial increase in frequency during the first scan, no further changes in the frequency response take place in subsequent scans (Fig. 4.19b).

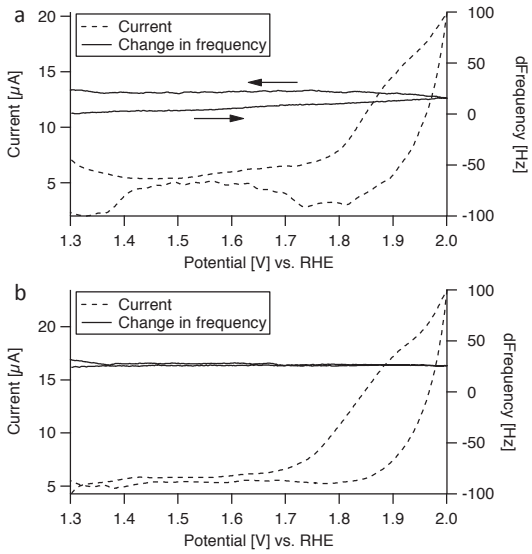

Figure 4.19: Results of EQCM experiments with 1.1 mM complex **1** in a 0.1 M $NaClO_4$ solution with a gold working electrode. Shown are the first scan (a) and the third scan (b) of a CV experiment, cycling the potential between 1.3 and 2.0 V vs. RHE at 1 mV/s, starting each scan at 1.3 V vs. RHE. The horizontal arrows indicate the direction of the scan.

*4.2.3 Electrochemistry of complex **3***

4.2.3a Cyclic voltammetry

The electrochemical behaviour of complex **3** was studied in both 0.1 M Na_2SO_4 and 0.1 M H_2SO_4 electrolyte solutions, using working electrodes made from gold, PG and ITO. However, preliminary experiments with an ITO working electrode gave poor results (Fig. C.3, Appendix C) which is most likely due to its nature as a semi-conductor. As a result, we refrained from in-depth investigations with this electrode material.

Considering the instability of gold oxide in the presence of halide ions (see chapter 2, Fig 2.2), electrochemical experiments of complex **3** in combination with a gold working electrode were limited to potentials below 1.3 V. Due to the lower contribution of the background current of a gold working electrode compared to a PG working electrode, CV experiments with a gold electrode were carried out below 1.3 V with the intention of obtaining a better visualization of the Fe^{II}/Fe^{III} redox couple. Figure 4.20a shows a voltammogram of complex **3** measured between 0.0 and 1.0 V, recorded with a gold working electrode in a 0.1 M H_2SO_4 solution. In the forward scan of the CV experiment, there are two oxidation waves visible between 0.6 V and 1.0 V whereas the reductive current in the backward scan appears as a single wave at 0.6 V. A voltammogram between 0.0 and 2.0 V,

recorded with a PG working electrode shows the same Fe^{II}/Fe^{III} redox behaviour, albeit less discernable due to the larger contribution of background current from the PG working electrode (Fig. 4.20b). Beyond that, the voltammogram shows an oxidative wave starting at 1.5 V with a sharp increase in current around 1.8 V.

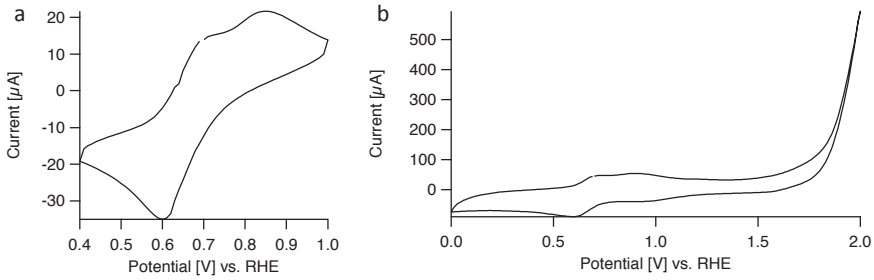

Figure 4.20: Voltammograms of 1.1 mM complex **3** in a 0.1 M H_2SO_4 solution. Shown are (a) the range between 0.4 and 1.0 V vs. RHE, starting at 0.7 V vs. RHE, recorded with a gold working electrode and (b) the range between 0.0 and 2.0 V vs. RHE, starting at 0.7 V vs. RHE recorded with a PG working electrode. Both voltammograms were recorded at a scan rate of 100 mV/s.

In a 0.1 M Na_2SO_4 electrolyte solution, qualitatively identical behaviour was observed for complex **3**, compared to the results obtained in a 0.1 M H_2SO_4 electrolyte solution. In the voltammogram recorded with gold in a 0.1 M Na_2SO_4 electrolyte solution, again two oxidation waves appear between 0.7 and 1.1 V in the forward scan. The backward scan again only shows a single reduction wave at 0.7 V (Fig. 4.21a). When scanning between 0.0 and 2.0 V at 100 mV/s with a PG working electrode, a single broad redox event between 0.7 and 1.1 V is resolved in both directions as well as an irreversible oxidative wave starting around 1.6 V(Fig. 4.21b).

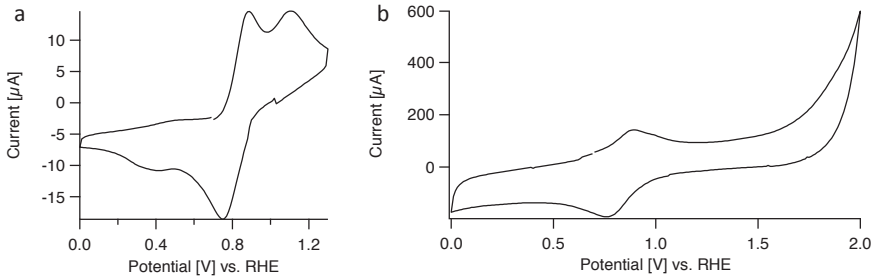

Figure 4.21: Voltammograms of 1.1 mM complex **3** in a 0.1 M Na_2SO_4 solution. Shown are (a) the range between 0.4 and 1.0 V vs. RHE, starting at 0.7 V vs. RHE, recorded with a gold working electrode and (b) the range between 0.0 and 2.0 V vs. RHE, starting at 0.7 V vs. RHE recorded with a PG working electrode. Both voltammograms were recorded at a scan rate of 100 mV/s.

The presence of two oxidation waves in the voltammograms indicates that a mixture of two species is present in solutions of complex **3**. This is in direct contrast to the results obtained for complexes **1** and **2** for which only a single $Fe^{II/III}$ redox couple was found. Considering the presence of chloride in the sample, one of the two oxidation peaks could be related to interactions of the metal centre with the chloride ions which are more strongly coordinating than triflate ions. However, the addition of several equivalents of sodium chloride to the electrolyte solution containing complex **3** does not result in a change in the corresponding voltammogram (Fig. 4.22).

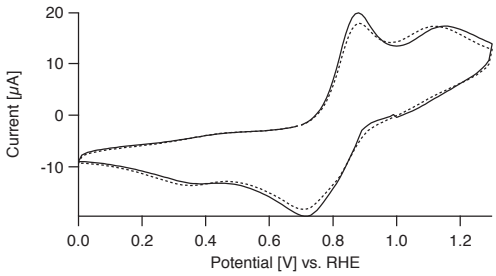

Figure 4.22: Voltammograms of 1.1 mM complex **3** in a 0.1 M Na_2SO_4 solution recorded with a gold working electrode. Shown are the result for 1.1 mM complex **1** (solid line) and 1.1 mM complex **3** + 9 equivalents of NaCl (dotted line). Both voltammograms were recorded between 0.0 and 1.3 V vs. RHE at a scan rate of 100 mV/s, starting at 0.7 V vs. RHE.

4.2.3b On-line electrochemical mass spectrometry

OLEMS experiments of complex **3** were carried out in both 0.1 M Na_2SO_4 and 0.1 M H_2SO_4 electrolyte solutions. The potential range of 1.3 to 2.0 V of the OLEMS experiments does not allow for the combination of complex **3** with a gold working electrode due to the instability of gold oxide in the presence of halide ions. Consequently, OLEMS experiments of complex **3** were performed exclusively with a PG working electrode. The results of the OLEMS experiments of complex **3** in a 0.1 M Na_2SO_4 solution (Fig. 4.23) are qualitatively similar to those obtained from OLEMS experiments of complex **1** in a 0.1 M $NaClO_4$ solution. In both cases, the current trace shows an oxidation wave, starting at about 1.5 V with a sharp increase in current starting near 1.8 V (Fig. 4.23, bottom). The *m/z* traces for both experiments show an onset of oxygen evolution around 1.8 V which correlates with the sharp increase in current. The onset of CO_2 formation (Fig. 4.23, middle) lies around 1.5–1.6 V, correlating with the onset of oxidative current in the current trace (4.23, bottom).

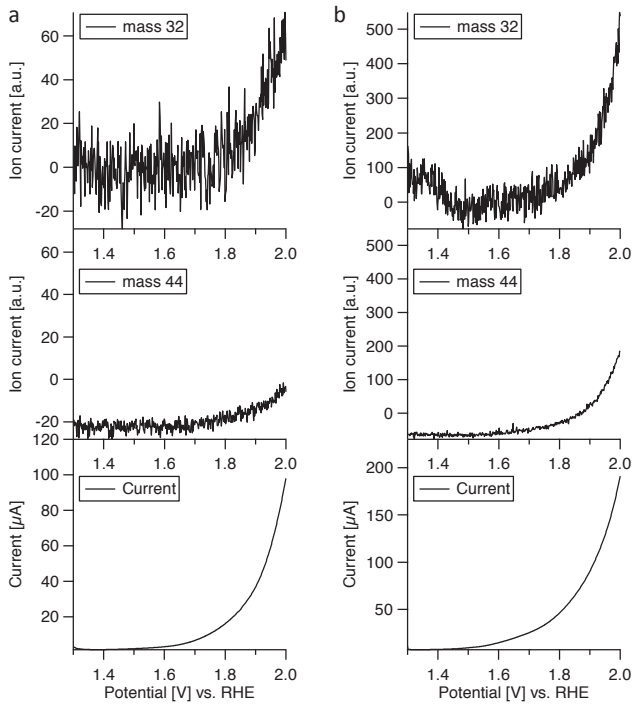

Figure 4.23: OLEMS measurements of (a) 1.1 mM complex **3** in a 0.1 M Na_2SO_4 solution and (b) 1.1 mM complex **1** in a 0.1 M $NaClO_4$ solution (cf. Fig. 4.13a). Both experiments were recorded with a PG working electrode, cycling the potential between 1.3 and 2.0 V vs. RHE, starting at 1.3 V vs. RHE at a scan rate of 1 mV/s. Depicted are the *m/z* traces of O_2 (top), CO_2 (middle) and the corresponding current (bottom). For the sake of clarity only the forward scan of each experiment is shown.

The OLEMS experiment of complex **3** in 0.1 M H_2SO_4 (Fig. 4.24) shows a behaviour that is qualitatively similar to that observed in 0.1 M Na_2SO_4. From 1.6 V onward, oxidative current can be seen in the current trace (Fig. 4.24, bottom) which correlates with the onset of CO_2 formation (Fig. 4.24, middle). The onset of oxygen evolution lies near 1.8 V (Fig. 4.24, top), correlating with a sharp increase in oxidative current visible in the current trace.

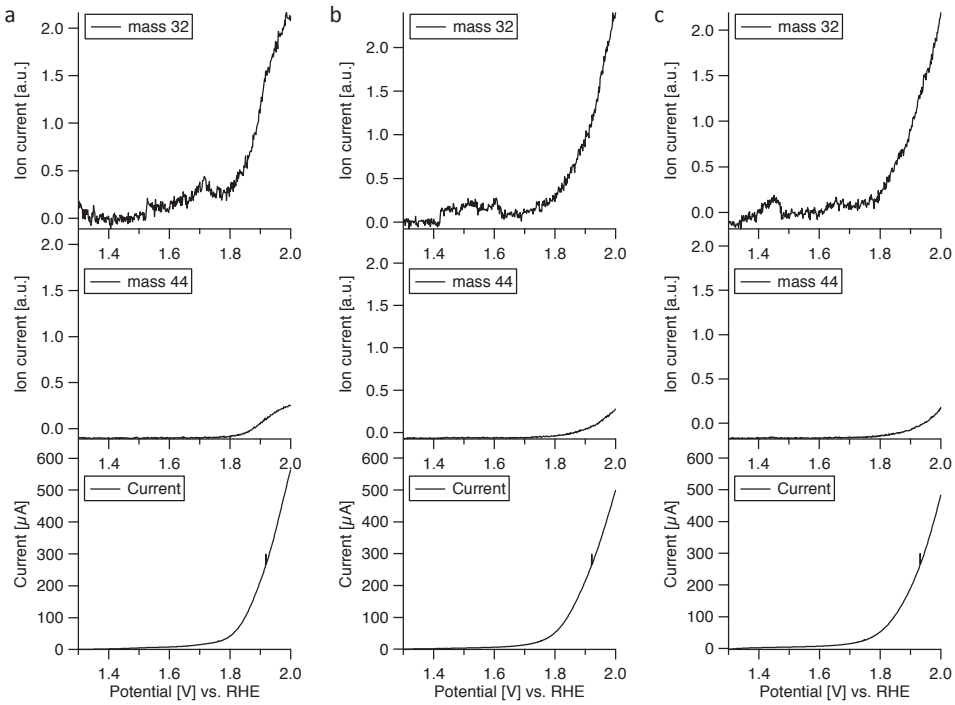

Figure 4.24: OLEMS measurement of 1.1 mM complex **3** in a 0.1 M H_2SO_4 solution using a PG working electrode, recorded while cycling the potential between 1.3 and 2.0 V vs. RHE, starting at 1.3 V vs. RHE at a scan rate of 1 mV/s. Depicted are the *m/z* traces of O_2 (top), CO_2 (middle) and the corresponding current (bottom). (a) scan 1 (b) scan 2 (c) scan 3. For the sake of clarity only the forward scan of each experiment is shown.

4.3 Discussion

One of the key research questions of this chapter was to investigate whether the significantly higher stability of complex **2** compared to complex **1** in experiments with chemical oxidants can also be observed during electrochemically driven water oxidation. Considering that the difference in turnover numbers between complexes **1** and **2** was found to be of the order of 4-5 in the presence of chemical oxidants, one would expect to find clear evidence for the increased robustness of complex **2** in the electrochemistry of both complexes if similar effects also play a role under electrochemical conditions. Instead, the results of cyclic voltammetry and on-line electrochemical mass spectrometry experiments showed that complexes **1** and **2** behave virtually identically in all experiments.

The electrochemistry of complexes **1** and **2** in combination with a PG working electrode is well behaved in the sense that no major changes were observed over time during electrochemical experiments. In CV experiments a single Fe^{II}/Fe^{III}

redox couple is observed at 0.9 V, followed by an irreversible oxidative wave starting at 1.5 V (Fig. 4.12) which could be assigned to a combination of oxygen evolution and CO_2 formation with an onset around 1.8 V for oxygen evolution and 1.5 V for CO_2 formation (Fig 4.13). Based on the OLEMS experiments with a PG working electrode alone, the source of the CO_2 cannot directly be determined unambiguously. The fact that very little CO_2 formation was observed during OLEMS experiments of complexes **1** and **2** with a gold working electrode, however (Fig. 4.14-4.16), suggests that the CO_2 formed during experiments with a PG electrode originates mainly from oxidation of the electrode material. In summary, the behaviour of complexes **1** and **2** in combination with a PG working electrode is consistent with a stable catalytic system.

When a gold working electrode is used instead of a PG electrode, the resulting electrochemistry of complexes **1** and **2** becomes significantly more complex. CV experiments between 0.0 and 2.0 V at 10 mV/s and OLEMS experiments between 1.3 and 2.0 V at 1 mV/s both showed a dynamic behaviour which evolved between scans for both complexes in combination with a gold working electrode.

In the CV experiment between 0.0 and 2.0 V an increase in the peak current can be seen with each scan (Fig 4.10-4.11 and Table 4.1). In contrast, the current recorded during the OLEMS experiments between 1.3 and 2.0 V does not show a significant increase in current at 2.0 V with each scan (Fig 4.14-4.16, bottom). This difference suggests that cycling over the gold oxidation and gold oxide reduction potential is a key factor for the increase in current at 2.0 V during prolonged potential cycling. However, in the OLEMS experiments with a gold working electrode, the current profile of the first scan is clearly different from the current profile of the second and third scan. The current trace of the first scan (4.16, bottom) shows the same two oxidation waves I and II between 1.5 and 1.9 V that were previously seen in CV experiments between 0.0 and 2.0 V (Fig. 4.9-4.10).

It is expected that the formation of gold oxide contributes at least to some extent to the oxidative current in the region between 1.3 and 2.0 V. In the CV experiment between 0.0 and 2.0 V, the gold oxide layer is reduced again in the backward scan of every cycle at potentials below 1.3 V which is why the same contribution from gold oxide formation is expected in every scan. In the OLEMS experiment between 1.3 and 2.0 V, however, the reduction of gold oxide is prevented since the potential never goes below 1.3 V. Therefore, the difference in the current profile between the first and the second scan of the OLEMS experiments is likely due to the formation of gold oxide during the first scan as the electrode was not oxidized

to gold oxide prior to the experiment. This hypothesis was confirmed by recording two back-to-back CV experiments between 1.3 and 2.0 V at 1 mV/s with a gold working electrode in the presence of complex **2**. Between both experiments, the electrode was exposed to new, unreacted complex while applying a resting potential of 1.3 V at the working electrode to prevent gold oxide reduction. Comparison of both CV experiments clearly shows that the oxidation waves I and II do not persist across experiments as long as gold oxide reduction is prevented (Fig. 4.17). Therefore the features must be related to gold oxidation processes at the electrode surface.

In the second and third scan of each OLEMS experiment with a gold working electrode, complex **1** and **2** both show a persistent behaviour which is comparable to what was observed in an OLEMS experiment with a PG working electrode. The current trace recorded with a gold working electrode shows a single oxidation wave, starting between 1.8 and 1.9 V while the O_2 mass trace shows oxygen evolution which correlates with the oxidative current (Fig. 4.14-4.15). The absence of any significant differences between the results of the second and third scan and the absence of CO_2 formation in both scans are again consistent with a stable catalytic system.

In contrast, the first scan of each OLEMS experiment of complex **1** or **2** with a gold working electrode gave different results for current, O_2 trace and CO_2 trace. While the difference in the current profile between the first scan of the OLEMS experiment and subsequent scans can largely be attributed to gold oxide formation processes at the working electrode, the mass traces of O_2 and CO_2 also show a different profile during the first scan compared to subsequent scans. The O_2 trace shows signs of oxygen evolution already at potentials as low as 1.6 V and the CO_2 trace shows signs of CO_2 formation from 1.8 V onward. These results might suggest that during the first scan a catalytically active species is present, giving rise to oxygen evolution starting at 1.6 V. This species might then undergo oxidative modification from 1.8 V onward, resulting in a different but stable species which is then catalytically active in the second and third scan with an onset of oxygen evolution around 1.9 V. However, as was already shown in the context of figure 4.17, exposing the electrode to new, unreacted complex between experiments does not recover the features of the first scan. While oxidative modification of the catalyst at high potentials could also explain the increasing current at 2.0 V in CV experiments between 0.0 and 2.0 V, this is

contradicted by the fact that the Fe^{II}/Fe^{III} redox couple does not appear to decrease (Fig. 4.11b and Table 4.1).

Another possible explanation for the difference between the first scan and subsequent scans of the OLEMS experiments could be the formation of minute amounts of catalytically active heterogeneous material at the electrode surface. However, EQCM experiments showed no signs of the formation of any deposit on the electrode surface. Instead, an increase in the frequency response at the gold working electrode was measured during the first scan of an EQCM experiment, recorded between 1.3 and 2.0 V at 1 mV/s in the presence of complex **1**, with no further change during the subsequent scans (Fig. 4.19). This observed increase in frequency is most likely not due to an actual decrease in the mass of the electrode. In previous reports, such behaviour has been attributed to the formation of bubbles at the surface of the electrode which lower the hydrostatic pressure of the electrolyte on the surface and result in an apparent decrease in mass.[17]

Based on the combined results of CV, OLEMS and EQCM experiments with complexes **1** and **2**, it appears unlikely that the changes between scans which were observed during the electrochemical experiments of both complexes with a gold working electrode are related to the formation of either a heterogeneous species or a modified homogeneous species from either complex. Instead all evidence points to the conclusion that all differences that are observed between scans are related to gold oxide formation and reduction processes at the electrode surface.

Complex **3** which was also studied using a PG working electrode showed the same qualitative oxygen evolution behaviour in an OLEMS experiment in a 0.1 M Na_2SO_4 electrolyte solution that was previously observed for complex **1** in a 0.1 M $NaClO_4$ electrolyte solution with a PG electrode. This result shows that – as expected – the oxidation state of the starting material does not influence the observed catalytic activity.

Despite the similarities in the electrochemistry of complexes **1**-**3**, complex **3** also showed clear differences from both other complexes. While complexes **1** and **2** only showed a single reversible Fe^{II}/Fe^{III} redox couple in a 0.1 M $NaClO_4$ electrolyte solution, complex **3** shows one reversible redox couple at 0.7 V and an irreversible oxidation wave between 1.0 and 1.2 V in a 0.1 M Na_2SO_4 electrolyte solution. The presence of two oxidation waves clearly indicates that a mixture of species is present in solutions of complex **3**. The addition of chloride to the electrolyte

solution containing complex **3** did not elicit any changes in the voltammogram, indicating that presence of two species is not related to coordination of chloride ions. Another possible explanation could be the *in situ* formation of other species upon dissolution such as a μ-OH bridged dimer.

The results of an OLEMS experiment with complex **3** in a 0.1 M Na_2SO_4 electrolyte solution reveal the same behaviour that was also found for the combination of complex **1** with a PG working electrode in a 0.1 M $NaClO_4$ electrolyte solution (Fig. 4.23). An OLEMS experiment of complex **3** in a 0.1 M H_2SO_4 electrolyte solution on the other hand gave results which appear to be qualitatively similar but quantitatively different from the results observed in a 0.1 M Na_2SO_4 electrolyte solution. However, these quantitative differences need to be interpreted carefully. The response in the mass traces will inevitably differ between experiments. This is due to the variability in the distance between the OLEMS tip and the working electrode on one hand and the inherent differences between two different OLEMS tips on the other hand. While the current that was recorded in both OLEMS experiments also strongly suggests a quantitative difference between both measurements, this difference in oxidative current is expected to be at least partially due to increased rates of CO_2 formation from the electrode material at acidic pH.[19-20]

4.4 Conclusions

The electrochemical behaviour of the α-Fe(bpmcn) complexes, which is described in this chapter, turned out to be substantially more complex than anticipated. All three complexes showed a comparable and persistent onset of oxygen evolution at around 1.8 V in OLEMS experiments with a PG working electrode. In contrast, the results of electrochemical experiments of complexes **1** and **2** with a gold working electrode depend strongly on the exact conditions. Considerable changes over time were observed during prolonged potential cycling between 0.0 and 2.0 V as well as going from the 1st to the 2nd scan of an OLEMS experiment. While all evidence suggests that these differences which evolve over time are related to gold oxide formation processes at the surface of the working electrode, the exact underlying mechanism remains unclear.

Even though catalytic water oxidation activity was found for all complexes examined in this chapter, the recorded onset potential of ~1.8 V is not outstanding compared to the other iron-based homogeneous water oxidation complexes reported in this thesis. This result is in direct contrast to the status of

the system as a benchmark catalyst when driven by chemical oxidants. Furthermore, complex **2** had previously been found to be 4-5 times more stable under Cerium(IV) conditions compared to complex **1** but no such major differences between the two complexes were found in electrochemical experiments. Instead, complexes **1** and **2** were found to behave virtually identically in all experiments, showing that other factors dominate in the electrocatalytical regime compared to catalysis driven by chemical oxidants.
Overall, the findings of this chapter highlight the importance of electrochemical studies for evaluating (potential) water oxidation catalysts as the results obtained in the presence of chemical oxidants cannot be reliably translated to electrochemistry. The results also show that the observed electrochemistry can vary significantly between two different electrode materials in the presence of the same catalyst.

4.5 Experimental

4.5.1 General

Complexes **1**-**3** were synthesized and characterized in the group of Miquel Costas at the University of Girona. The complexes were used as received.
Complexes **1** and **2** were stored under argon in a glovebox to prevent oxidation in air.

4.5.2 Electrochemical experiments

All electrochemical measurements with the exception of the EQCM experiments (details below) were performed in a custom made single-compartment glass cell on Ivium potentiostats, operated by IviumSoft software, using a three-electrode setup. The working electrodes were a pyrolytic graphite (PG) disc with a (geometric) surface area of 0.20 cm^2 and a gold disc with a (geometric) surface area of 0.13 cm^2. For the experiments with an ITO working electrode, a small slice of ITO covered glass (ca. 0.5x1.5 cm) was used. While the gold and PG working electrodes were used in hanging meniscus configuration, the ITO electrode was partially submerged in the electrolyte solution. A large surface area gold plate was used as a counter electrode. The reference electrode was a reversible hydrogen electrode (RHE) made up of a platinum mesh in H_2-saturated electrolyte at the same pH as the working solution. The cell and the reference electrode were connected via a Luggin capillary. A fresh PG surface was prepared before each

experiment by polishing the working electrode with sandpaper and subsequent removal of excess debris by sonication in Milli-Q water for at least 5 minutes.
The gold electrode was prepared before each experiment by oxidizing the surface at 10 V for 30 s in a 10% H_2SO_4 solution, followed by stripping of the gold oxide layer in a 6 M HCl solution and subsequent electro-polishing of the electrode by scanning for 200 cycles between 0.0 and 1.75 V vs. RHE at 1000 mV/s in a 0.1 M $HClO_4$ electrolyte solution.
All glassware used in electrochemical measurements was routinely cleaned of any organic contamination by boiling in 3:1 mixture of concentrated sulfuric and nitric acid. Prior to each experiment the glassware was cleaned by threefold rinsing and boiling in Milli-Q water. The electrolyte solutions were prepared from p.a. grade chemicals obtained from Merck (Suprapur®) and Milli-Q water.
Prior to measurements, the electrolyte solution was purged of air by bubbling with argon (Linde, Ar 6.0) for at least 20 minutes. During the measurements, the cell was constantly kept under argon flow to prevent air from entering.
For the OLEMS measurements, the gasses formed at the working electrode were collected via a hydrophobic tip (KEL-F with a porous Teflon plug) in close proximity to the surface of the working electrode and analyzed in a QMS 200 mass spectrometer. A detailed description of the OLEMS setup is available elsewhere.[8]
All electrochemical potential cycling in combination with OLEMS was done at a scan rate of 1 mV/s. For the mass spectrometry data recorded via OLEMS during cylic voltammetry measurements, background correction was done by assuming an exponential decay fit (concerns Figures 4.13, 4.14, 4.15, 4.16, 4.18, 4.23 and 4.24).
EQCM experiments were performed in a 3 mL Teflon cell purchased from Autolab. The top part of the cell was modified to allow for electrochemical measurements under an inert atmosphere. For further details, see appendix B (Fig. B.9). The EQCM was controlled by an Autolab potentiostat operated by NOVA 2.0 software. Autolab EQCM electrodes with a surface area of 1.5 cm^2 consisting of a 200 nm gold layer deposited on a quartz crystal were used as working electrodes. A custom made RHE reference electrode was used which is described elsewhere.[9]

4.5.3 Sample preparation

Samples of complexes **1** and **2** were weighed in an argon atmosphere inside the glovebox and stored in a closed vessel. Prior to the experiment, the complexes were dissolved in a small amount of electrolyte solution (typically 1-2 mL) taken

from the cell which had previously been purged with argon and subsequently added to the electrochemical cell. The electrolyte solution was then purged again by bubbling with argon for several minutes.
Samples of complex **3** were weighed in air and subsequently added to the cell in a manner analogous to that described for complexes **1** and **2**.
For all electrochemical experiments a 1.1 mM concentration of catalyst was used unless stated otherwise.

4.6 Supporting Info

The following supplementary information can be found in Appendix C: A depiction of the flocculent white precipitate formed as a result of the decomposition of complex **1** at pH 1 inside the electrochemical cell (Fig. C.1), an illustration of the artefacts routinely found in the *m/z* signals during OLEMS measurements (Fig. C.2 and Fig. C.3) and a voltammogram of complex **3** recorded with an ITO working electrode (Fig. C4).

4.7 References

[1] J. L. Fillol; Z. Codola; I. Garcia-Bosch; L. Gomez; J. J. Pla; M. Costas, *Nat. Chem.* **2011**, *3*, 807-813.
[2] T. J. Collins, *Acc. Chem. Res.* **1994**, *27*, 279-285.
[3] W. C. Ellis; N. D. McDaniel; S. Bernhard; T. J. Collins, *J. Am. Chem. Soc.* **2010**, *132*, 10990-10991.
[4] M. Costas; J. L. Fillol, *Personal communication*, **2017**.
[5] S. L. Esarey; J. C. Holland; B. M. Bartlett, *Inorg. Chem.* **2016**, *55*, 11040-11049.
[6] D. Hong; S. Mandal; Y. Yamada; Y. M. Lee; W. Nam; A. Llobet; S. Fukuzumi, *Inorg. Chem.* **2013**, *52*, 9522-9531.
[7] O. Diaz-Morales; T. J. Hersbach; D. G. H. Hetterscheid; J. N. Reek; M. T. M. Koper, *J. Am. Chem. Soc.* **2014**, *136*, 10432-10439.
[8] A. H. Wonders; T. H. M. Housmans; V. Rosca; M. T. M. Koper, *J. Appl. Electrochem.* **2006**, *36*, 1215-1221.
[9] P. Abril; M. P. del Río; C. Tejel; T. W. G. M. Verhoeven; J. W. H. Niemantsverdriet; C. J. M. Van der Ham; K. G. Kottrup; D. G. H. Hetterscheid, *ACS Catal.* **2016**, *6*, 7872-7875.
[10] S. Fukuzumi; D. Hong, *Eur. J. Inorg. Chem.* **2014**, *2014*, 645-659.
[11] U. Hintermair; S. W. Sheehan; A. R. Parent; D. H. Ess; D. T. Richens; P. H. Vaccaro; G. W. Brudvig; R. H. Crabtree, *J. Am. Chem. Soc.* **2013**, *135*, 10837-10851.
[12] B. Limburg; E. Bouwman; S. Bonnet, *Coord. Chem. Rev.* **2012**, *256*, 1451-1467.
[13] G. Chen; L. Chen; S. M. Ng; W. L. Man; T. C. Lau, *Angew. Chem., Int. Ed.* **2013**, *52*, 1789-1791.

[14] Y. Lin; S. Zhou; S. W. Sheehan; D. Wang, *J. Am. Chem. Soc.* **2011**, *133*, 2398-2401.
[15] M. T. Mayer; C. Du; D. Wang, *J. Am. Chem. Soc.* **2012**, *134*, 12406-12409.
[16] K. M. H. Young; B. M. Klahr; O. Zandi; T. W. Hamann, *Catal. Sci. Technol.* **2013**, *3*, 1660.
[17] N. D. Schley; J. D. Blakemore; N. K. Subbaiyan; C. D. Incarvito; F. D'Souza; R. H. Crabtree; G. W. Brudvig, *J. Am. Chem. Soc.* **2011**, *133*, 10473-10481.
[18] C. J. M. van der Ham; F. Işık; T. W. G. M. Verhoeven; J. W. Niemantsverdriet; D. G. H. Hetterscheid, *Catal. Today* **2017**, *290*, 33-38.
[19] K. G. Gallagher; T. F. Fuller, *Phys. Chem. Chem. Phys.* **2009**, *11*, 11557-11567.
[20] Y. Yi; G. Weinberg; M. Prenzel; M. Greiner; S. Heumann; S. Becker; R. Schlögl, *Catal. Today* **2017**, *295*, 32-40.